MULTIFREQUENCY OBSERVATIONS

R. Glitz, F. Heel, H. Kietzmann, H. Öttl, and C. Schmullius

1. Introduction

Analyses of SAR image data were performed at DLR to classify various kinds of vegetation and different terrain types. The data were collected both with the DLR experimental synthetic aperture radar (E-SAR) in X-band, C-band and L-band and with the NASA/JPL DC-8 SAR in C-band, L-band and P-band.

E-SAR is a single frequency and single polarization system (both parameters can be selected) but several flights were used to collect multifrequency/multipolarization data which were geometrically matched after processing. Classification of different crop types was based on comparison of the backscatter coefficients of calibrated SAR data in different frequency bands and polarizations.

The DC-8 SAR collects polarimetric data in different bands simultaneously. Data acquired with the NASA/JPL DC-8 SAR are qualified for scientific investigations by reducing the cross-talk and channel imbalance to a tolerable extent. The data are absolutely calibrated by using reference targets with known backscattering cross-sections. The signatures and polarimetric features of terrain types, such as grassland, concrete, sea, forest (coniferous; deciduous) and urban areas, are extracted and discussed with respect to frequency and incidence angle dependence. A multifrequency polarimetric feature vector was applied for classification. The results of this new approach for separating and classifying different object classes are presented here.

2. Crop Classification Based on E-SAR Data

During the Multi-Sensor Airborne Campaign (MAC) Europe '91 on July 12th, the test site Oberpfaffenhofen was covered by E-SAR flights in order to collect X-HH, X-VV and C-VV SAR data.

The latest capabilities of the DLR E-SAR are described in [1], and the results of the MAC '91 agricultural classification in [2]. The high spatial resolution of E-SAR (2 to 3 m) allowed even the analysis of small fields with very good results. An unsupervised migrating means classification (k-distribution) resulted in a rejection of only about 5 % of the observed area.

On May 20th, 1992, another airborne campaign was performed with the E-SAR, after it had been modified to provide an additional L-band capability. L-HH, C-VV, X-VV, and X-HH data were collected. A selected agricultural test site is shown in Fig.1 corresponding to these four data sets.

It should be mentioned that the spatial resolution of the L-HH image is lower than in C-band and X-band images. The approximately equally spaced white spots in the images represent electric pylons. Test site statistics of the six main crop types are illustrated as scatter grains in Fig. 2 for C-VV and X-VV and in Fig. 3 for L-VV and C-VV. The ellipses include ± 1 standard deviation around the mean.

The plots in Fig. 2 permit a proper discrimination of the various crop types, while Fig. 3 only shows small differences in L-band for a number of crops. This observation is valid for the vegetation in late May.

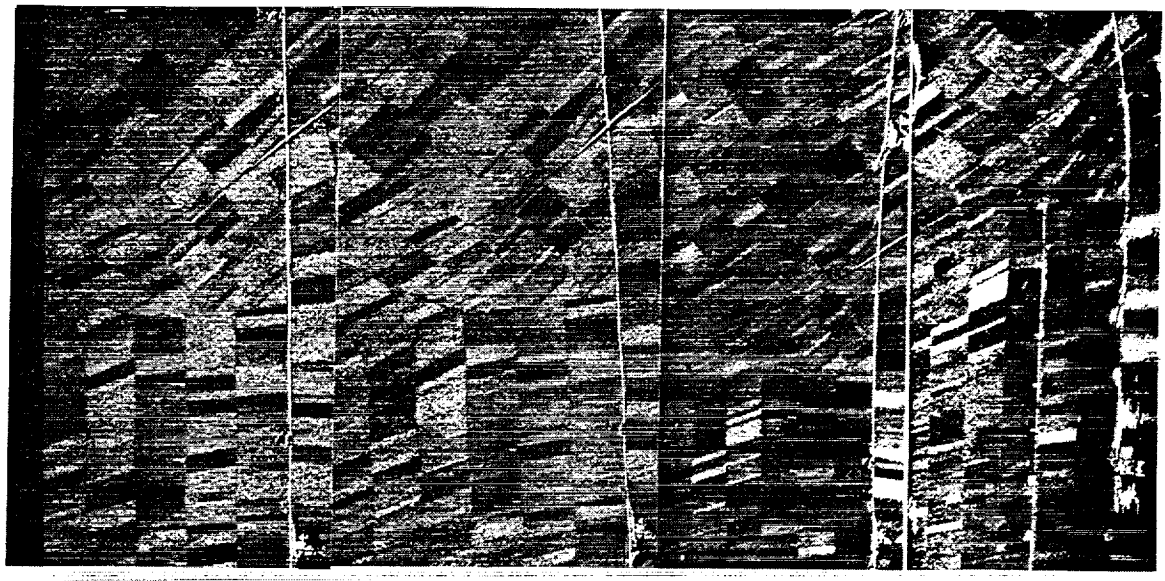

Fig. 1: Top: The SAR images based on X-HH, X-VV, C-VV and L-HH data.
Bottom: Color composite image consisting of the following co-registered channels: L-HH (red), X-VV (green), and C-VV (blue).

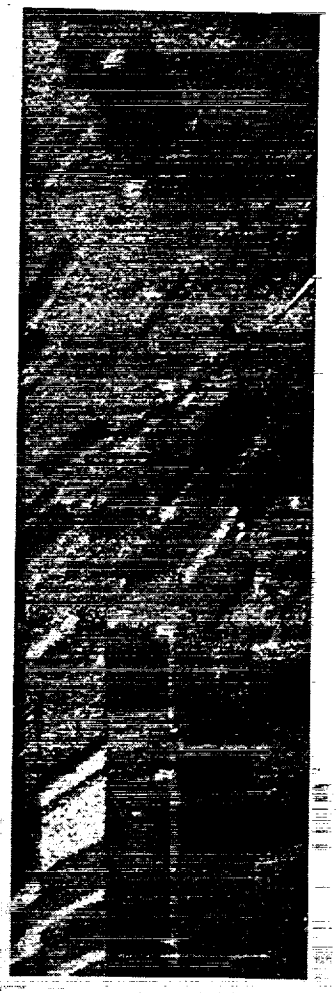

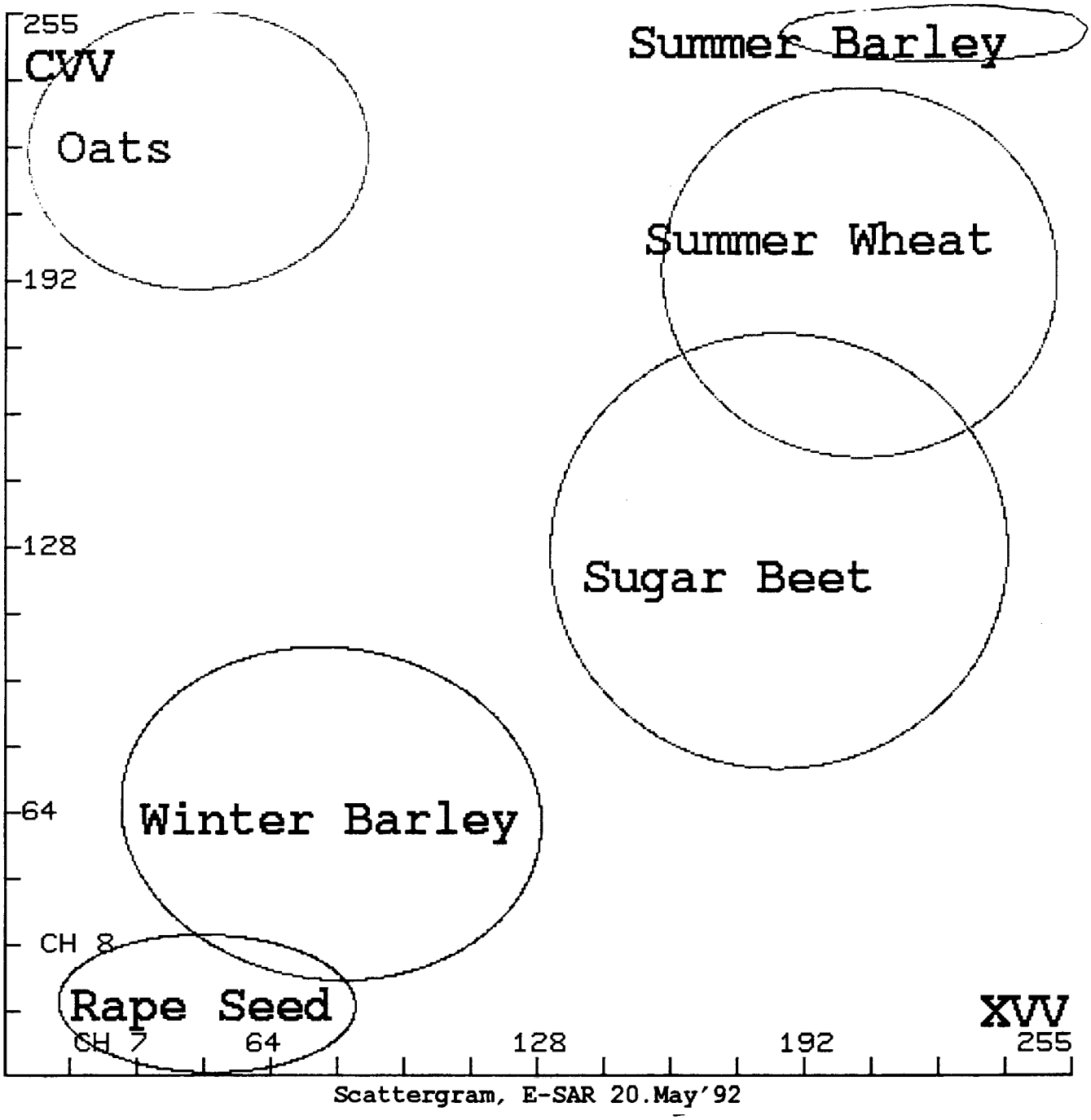

Fig. 2: Scattergram of C-VV versus X-VV bands showing proper crop type discrimination.

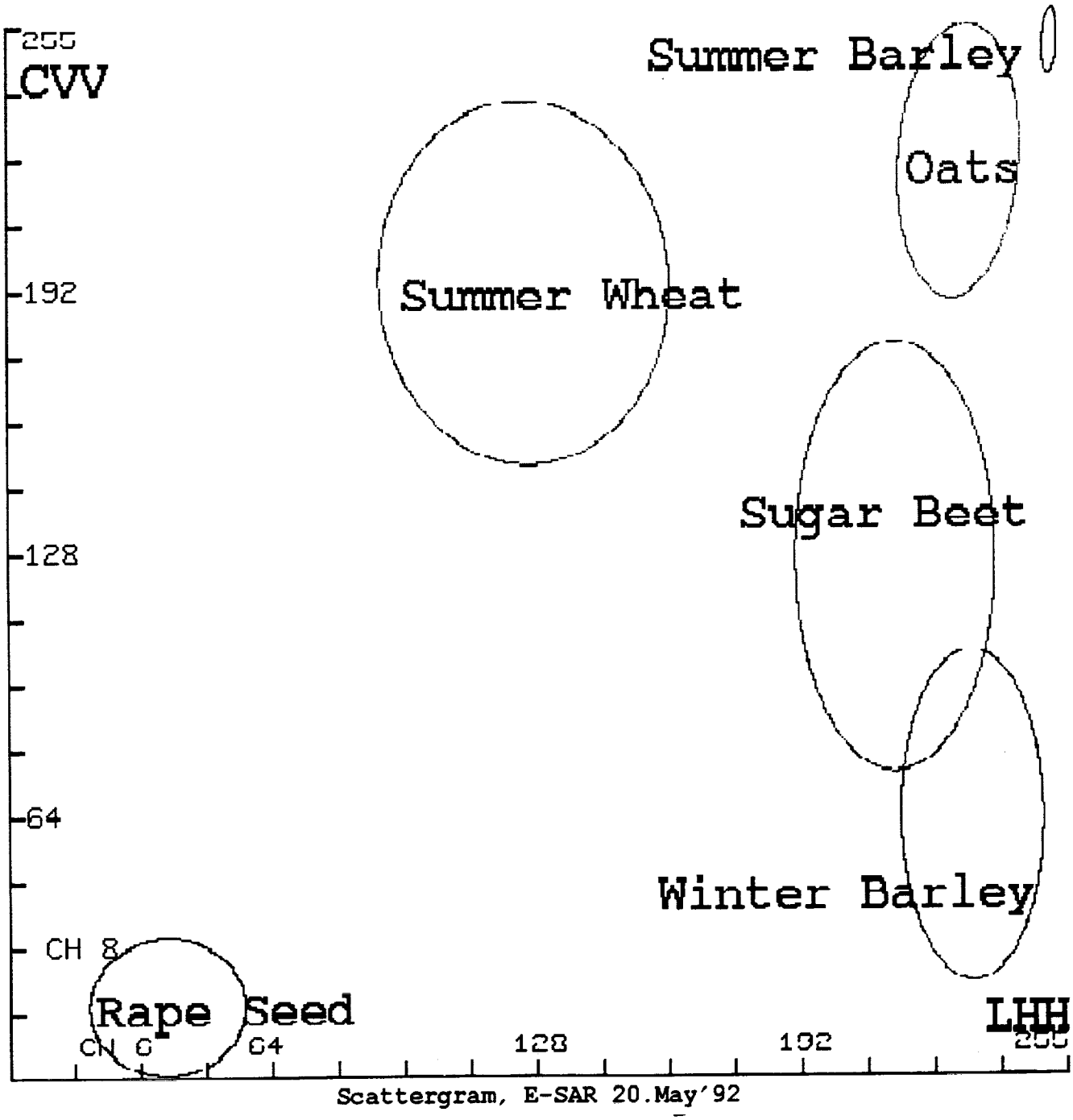

Fig. 3: Scattergram of C-VVversus L-HH bands showing overlapping crop type statistics in the L-band.

3. Airborne Campaign with the NASA/JPL DC-8 SAR

In August 1989, an airborne SAR measurement campaign took place at the Oberpfaffenhofen (OP) test site area. The NASA/JPL DC-8 SAR system is equipped with three simultaneously operating SAR sensors, comprising C-, L- and P-band with wavelengths of 5.6 cm, 24 cm and 68 cm [3]. This system permits fully polarimetric measurements [4] which means acquiring the scattering matrix elements HH, HV, VH and VV. Three parallel tracks were flown to cover scenes of the same area under different incidence angles of 35°, 45°, and 55°.

In order to qualify these multifrequency data products for comprehensive signature analysis, the appropriate preprocessing had to be carried out [5]. The data prepared in this way, with their diversity in frequency, incidence angle and polarization states, form a good basis for signature and classification studies.

4. Data Preparation and Terrain Type Selection

JPL delivered single look complex SAR image data. These fully polarimetric data covered the P-, L- and C-frequency bands and had been radiometrically corrected.

As a first step to qualify all the data products for signature analysis, polarimetric calibration (cross-talk, channel imbalance) was performed at the Institute for Radiofrequency Technology followed by absolute calibration [6], [7]. Finally, the data were transformed to a 4-look image format.

After adequate image data preparation, a total power C-band image (Fig.4) representing the central part of the Oberpfaffenhofen test site area (12.5 km x 5 km) was selected for terrain type investigations. This image includes the contours of the specific terrain types to be analysed, such as grassland (W1, W2), concrete (B1, B2), lake water surface (S1, S2), coniferous forest (N1, N2), deciduous forest (L1, L2) and urban areas (A1, A2). The terrain type sizes vary from about 10 000 m^2 to 30 000 m^2 depending on the availability of the corresponding terrain types.

5. Multifrequency Terrain Type Signatures and Classification

The simultaneous P-, L- and C-band measurements of each selected terrain type enabled the study of their backscattering behaviour. Fig. 5 shows the comparison of their copolarized backscattering coefficients σ°_{hh}. It is generally seen that urban areas and forests give rise to considerably higher returns than grass, concrete or lake targets. This can be explained by an increased roughness and reflection-like interactions. As expected for surface targets, especially in the case of grassland, a σ°_{hh} decrease could be found in the C-L-P sequence. An inversion of this sequence can be recognized for all forest areas. C-band signals mainly interact with needles or leaves in the upper forest region. Medium sized twigs and branches predominantly scatter the L-band signals, and the P-band signals couple essentially with the larger branches and trunks. This demonstrates that the size of the scattering elements considerably influences the target return. The urban area data show no significant wavelength dependence because of similar scattering mechanisms for the aforementioned frequencies.

The corresponding copolar phase differences are shown in Fig. 6. We recog-

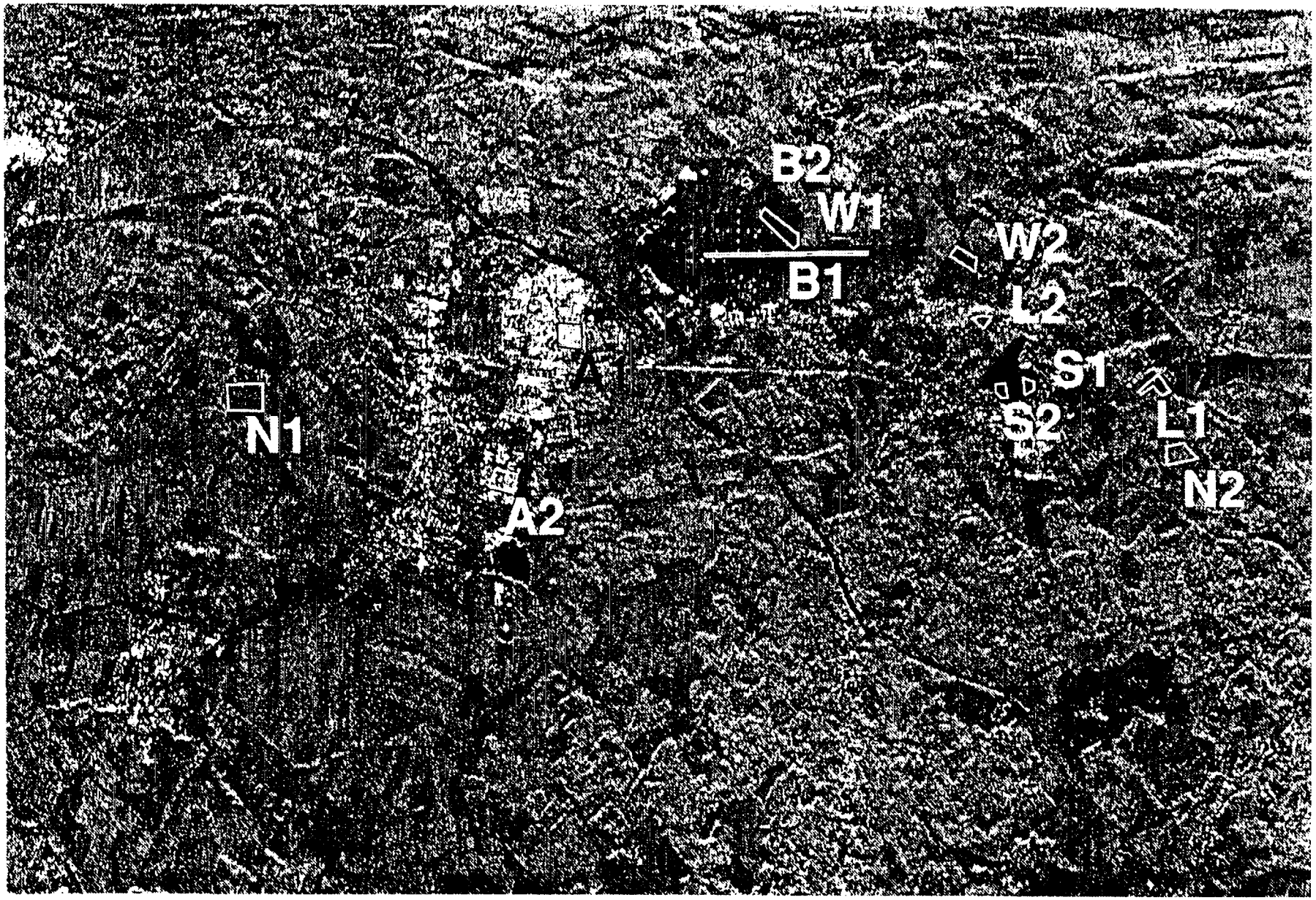

Figure 4: Total power C-band image with selected terrain types

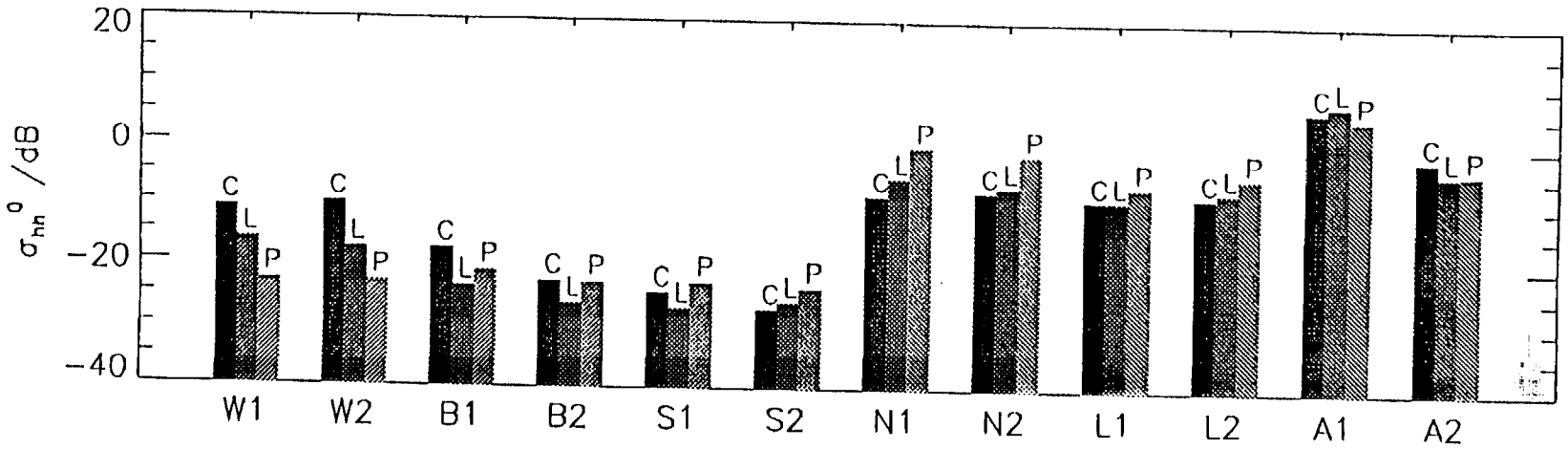

Figure 5: Backscattering coefficient σ_{hh}^{o} for P-,L- and C-Band.

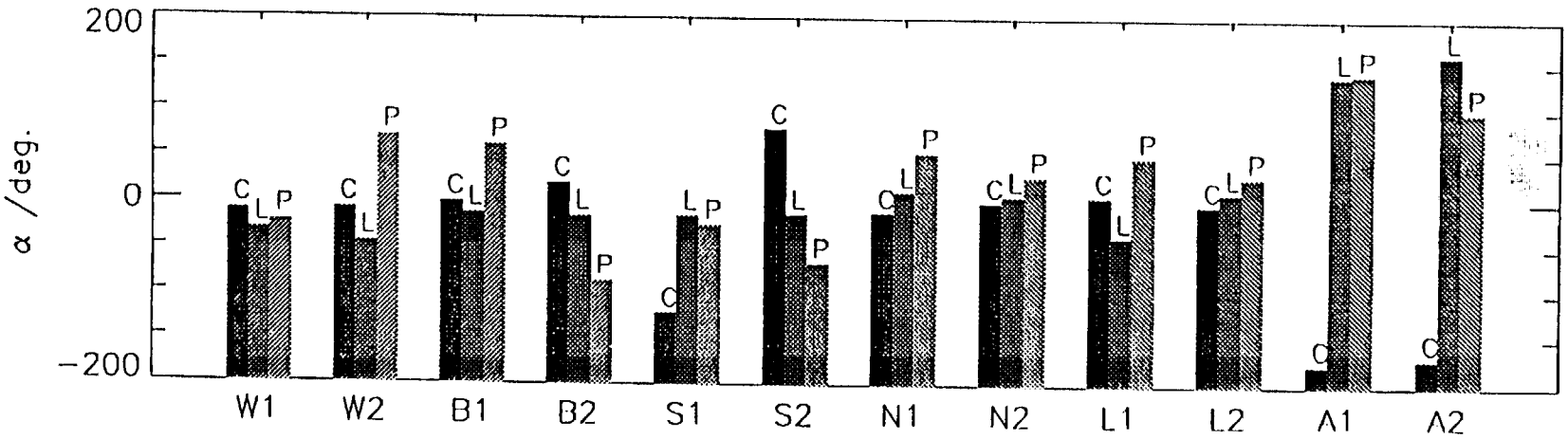

Figure 6: Copolar phase difference α for P-,L- and C-Band.

nize a phase difference for urban areas of approximately ±180°, indicating a relatively clear double bounce scattering in contrast to all analysed surface type targets. In the case of concrete and lake areas, there are some phase anomalies due to interferences from stronger targets. Regarding forests, the phase increases with increasing wavelength due to scattering mechanisms, as shown in Fig. 6.

Further investigations deal with the influence of the incidence angle on the backscattering coefficient σ°_{hh} of coniferous and deciduous (Fig. 7) forests. For coniferous forest, a clear decrease in σ°_{hh} is observed in the incidence angle range from 40° to 50° for all concerned wavelengths, whereas deciduous forest shows this dependence only for C-band. This latter target type reveals no obvious incidence angle variation of σ°_{hh} for P- and L-band which could be explained by the orientation of branches and twigs in this angle range. The σ°_{hh} behaves like that of a rough surface consisting of a layer of needles or leaves. The bars in Fig. 7 indicate the standard deviation around the mean values.

A statistical procedure [5] has been developed, based on the maximum-likelihood method, to take into account the ramdomness of distributed targets.

Analyses of a variety of polarimetric quantities allow the extraction of the most significant components to establish a multifrequency polarimetric feature vector. This feature vector consists of the scattering amplitudes HH,

VV, HV and the HH/VV phase difference for the applied P-, L- and C-band frequencies resulting in a total of twelve dimensions. In order to meet the statistical nature of each terrain class of interest, the mean and the covariance have to be determined for the single features and the overall feature vector. Adequate processing of this feature representation permits a separation of different terrain classes depending on their specific scattering properties. Thus, a procedure is established for classifying different terrain types. Fig. 8 illustrates a classification result extracted from the scene in Fig. 4 concerning coniferous forests. The black areas in the scene are classified as coniferous forest. The corresponding test areas N1 and N2 are correctly assigned whereas negligible misclassification occurs in all other test areas. Results with similar quality have also been obtained for other terrain classes.

6. Conclusions

The comparison with ground truth observations shows that terrain classification from calibrated radar image data in different frequency bands exhibits a high degree of reliability. The amplitude relationship of backscattered signals in X-band and C-band contains sufficient information for crop classification.

In general, for the classification of different terrain types, the use of a multifrequency polarimetric feature vector showed promising results. The large number of degrees of freedom associated with this vector allows an increased variety of signature investigations.

Therefore, to enhance the potential of remote sensing, such methods should be further investigated and applied in the future.

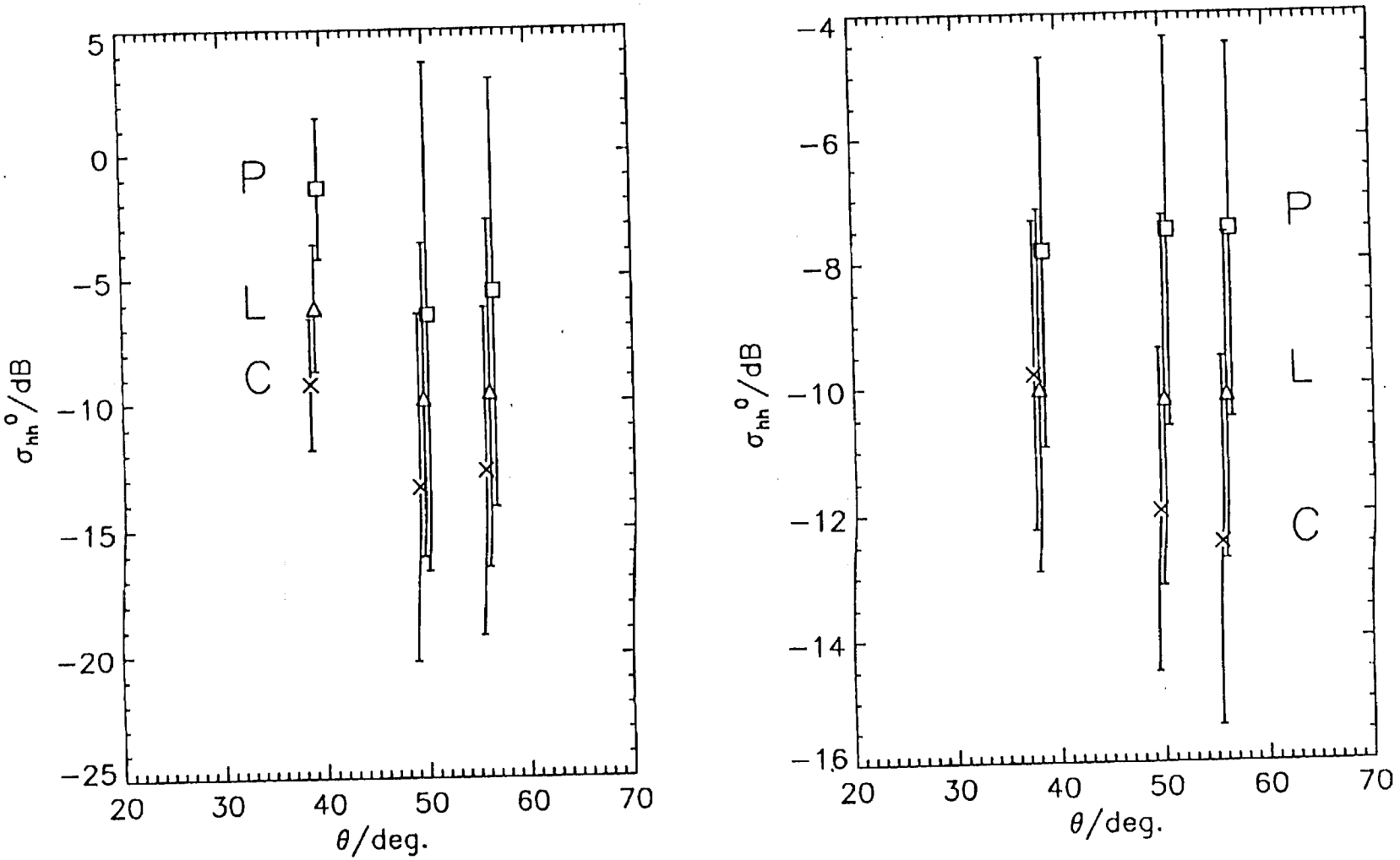

a. coniferous forest N1

b. deciduous forest L1

Figure 7: Backscattering coefficient σ^o_{hh} versus incidence angle Θ.

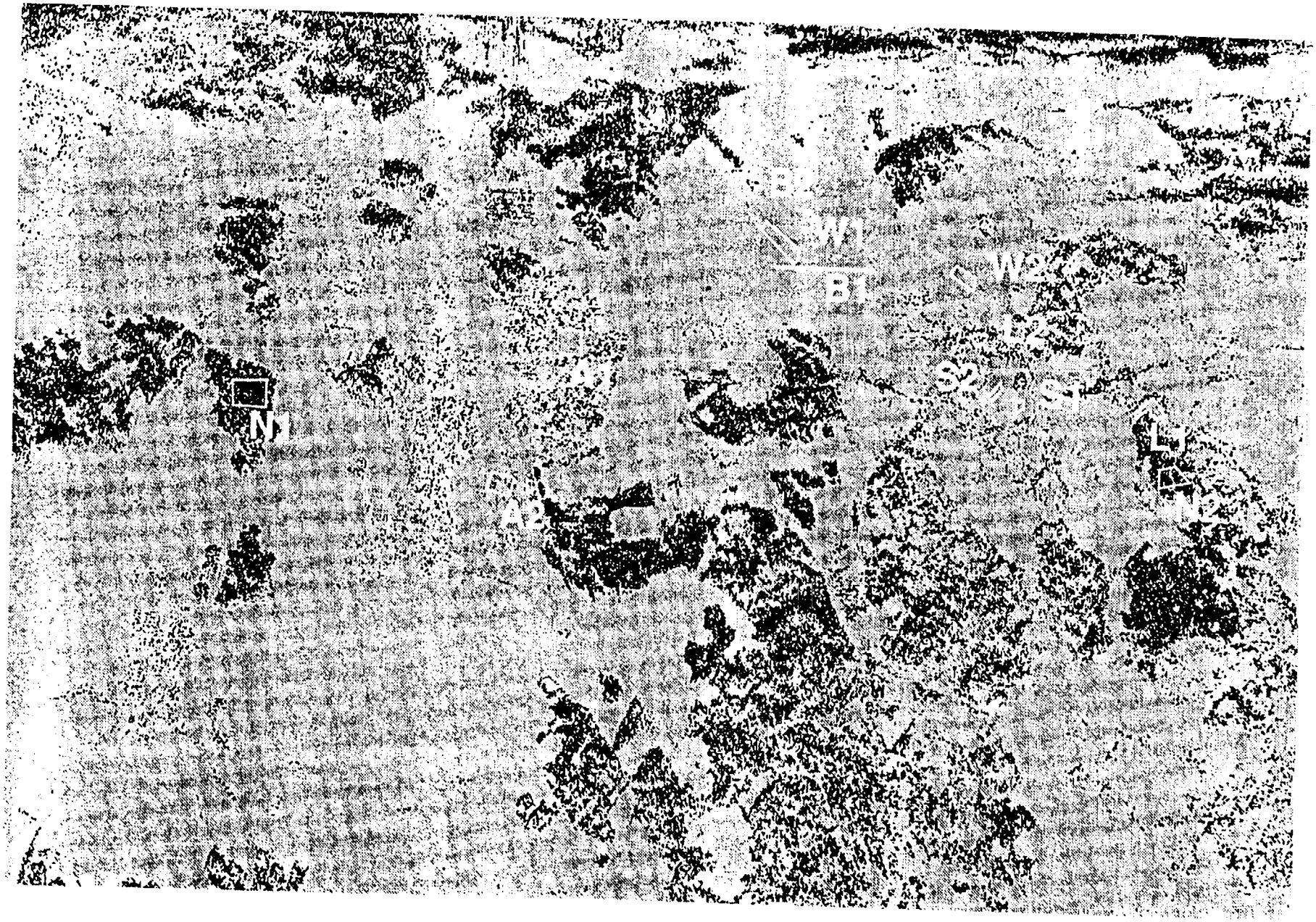

Figure 8: Coniferous forest classification image.

5. References

[1] Horn, R. et al. — A Refined Procedure to Generate Calibrated Imagery from Airborne Synthetic Aperture Radar Data.

Will be published 1993 in IEEE Trans. on Geosc. and Rem. Sens.

[2] Schmullius, C., Nithack, J. — High-Resolution SAR Frequency and Polarization Dependent Backscatter Variations from Agricultural Fields,

Proc. IGARSS '92, 26-29 May, Houston, pp. 930-932.

[3] Held, D.N. et al. — The NASA/JPL Multifrequency, Multipolarization Airborne SAR System.

Proc. IGARSS '88, pp. 345-350, Edinburgh, Scotland, Sept. 1988.

[4] Evans, D.L. et al. — Radar Polarimetry: Analysis Tools and Applications.

IEEE Trans. on Geoscience and Remote Sensing, Vol. 26, pp. 774-789,(1988).

[5] Glitz, R. — The Use of Polarimetric Multifrequency SAR for Characterizing Terrain Classes.

Proc. of the Central Symposium of the 'International Space Year' Conf., Vol. II, pp. 411-418, Munich, Germany, March 30 - April 4, 1992.

[6] Van Zyl, J.J. — Calibration of Polarimetric Radar Images Using only Image Parameters and Trihedral Corner Reflector Responses.

IEEE Trans. on Geoscience and Remote Sensing.

[7] Zink, M., Heel, F. Kietzmann, H. — The Oberpfaffenhofen SAR Calibration Experiment of 1989.

Journal of Electromagnetic Waves and Application, Vol. 5, No. 9, pp 935-951, 1991.

Submit

THE NEED FOR RADAR SIGNATURE MEASUREMENTS

Alois J. Sieber, Carlo Lavalle
Institute for Remote Sensing Applications
Joint Research Centre
I–21020 Ispra – Italy

Parameters which are characteristic for selected objects are known as signatures for these objects. As an example one may think about the handwriting as being such a characteristic signature for the individual writer. One important task in working with radar data is to search for information about targets of interest which are unique for these objects. However, previous work with air– and spaceborne radar images demonstrated that the resulting object information does not only depend on the prime measurement parameters like the frequency, the polarization and the illumination geometry adopted in the measurement. Further important effects are due to the illumination technique, the length of the synthetic aperture or the changing illumination angle throughout the synthetic aperture, the bandwidth and,as a consequence, it seems that each system, air or space–borne, shows different object features.

The upcoming two years will provide for the first time unique opportunities to compare target information collected almost simultaneously over the identical sites by SAR systems on the successfully working ERS–1 of ESA, the Japanese ERS–1, the unique multi–temporal Shuttle Imaging Radar (SIR) programme, the NASA/JPL multiparameter AIRSAR, the Canadian multi parameter SAR sensor of the CCRS and INTERA, the European multi–parameters SAR sensor EARSEC as well as many ground based radar systems in different parts of the covered part of the earth. All these data collection efforts will be complemented by a device dedicated to radar signature measurements under fully controlled environmental conditions, the European Microwave Signature Laboratory (EMSL).

The paper will present a systematic approach to investigate the signatures of selected objects using controlled experiments and translating them into the real world by physically sound models.

While in–field experiments are locally fixed, while air–borne measurements are regionally bound and while space–borne systems are often discussed in the frame of global issues, the multi–parameters Shuttle Imaging Radar programme is a perfect tool for the data collection of geophysically calibrated radar signature on a large scale – if the interpretation of its data is physically based and supported by controlled signature measurements. The paper will demonstrate that the Shuttle Imaging Radar (SIR) programme and the work in the European Microwave Signature Laboratory (EMSL) are complementing each other and are linked by the North American and the European airborne SAR systems.

FUTURE PROGRAMS